Acta Crystallographica Section B
Structural Science
ISSN 0108-7681

Crystal chemistry of transition metal diarsenates $M_2As_2O_7$ (M = Mn, Co, Ni, Zn): variants of the thortveitite structure

Matthias Weil* and Berthold Stöger

Institute for Chemical Technologies and Analytics, Division of Structural Chemistry, Getreidemarkt 9/164-SC, A-1060 Vienna, Austria

Correspondence e-mail: mweil@mail.zserv.tuwien.ac.at

Received 14 July 2010
Accepted 11 October 2010

The structures of the 3*d* divalent transition-metal diarsenates $M_2As_2O_7$ (M = Mn, Co, Ni, Zn) can be considered as variants of the monoclinic ($C2/m$) thortveitite [$Sc_2Si_2O_7$] structure type with $a \simeq 6.7$, $b \simeq 8.5$, $c \simeq 4.7$ Å, $\alpha \simeq 90$, $\beta \simeq 102$, $\gamma \simeq 90^\circ$ and $Z = 2$. $Co_2As_2O_7$ and $Ni_2As_2O_7$ are dimorphic. Their high-temperature (β) polymorphs adopt the thortveitite aristotype structure in $C2/m$, whereas their low-temperature (α) polymorphs are hettotypes and crystallize with larger unit cells in the triclinic crystal system in space groups $P\bar{1}$ and $P1$, respectively. $Mn_2As_2O_7$ undergoes no phase transition and likewise adopts the thortveitite structure type in $C2/m$. $Zn_2As_2O_7$ has an incommensurately modulated crystal structure [$C2/m(\alpha,0,\gamma)0s$] with $\mathbf{q}$ = [0.3190 (1), 0, 0.3717 (1)] at ambient conditions and transforms reversibly to a commensurately modulated structure with $Z = 12$ ($I2/c$) below 273 K. The Zn phase resembles the structures and phase transitions of $Cr_2P_2O_7$. Besides descriptions of the low-temperature $Co_2As_2O_7$, $Ni_2As_2O_7$ and $Zn_2As_2O_7$ structures as five-, three- and sixfold superstructures of the thortveitite-type basic structure, the superspace approach can also be applied to descriptions of all the commensurate structures. In addition to the ternary $M_2As_2O_7$ phases, the quaternary phase $(Ni,Co)_2As_2O_7$ was prepared and structurally characterized. In contrast to the previously published crystal structure of the mineral petewilliamsite, which has the same idealized formula and has been described as a 15-fold superstructure of the thortveitite-type basic structure in space group $C2$, synthetic $(Ni,Co)_2As_2O_7$ can be considered as a solid solution adopting the α-$Ni_2As_2O_7$ structure type. Differences of the two structure models for $(Ni,Co)_2As_2O_7$ are discussed.

1. Introduction

Divalent metal diarsenates(V)[1] have the general formula $M_2As_2O_7$. For this family numerous phases have been structurally determined to date. The structures with M = Mg (single-crystal X-ray data: Lukaszewicz, 1963; Calvo & Neelakantan, 1970), Ca (single-crystal X-ray data: Pertlik, 1980), Cd (single-crystal X-ray data: Weil, 2001), Mn (neutron powder data: Buckley *et al.*, 1990; X-ray powder data: Aranda *et al.*, 1991) and the high-temperature polymorphs of the transition metals Co, Ni (neutron powder data: Buckley *et al.*, 1990) and Cu (X-ray powder data: Weil *et al.*, 2004*a*) adopt the monoclinic thortveitite [$Sc_2Si_2O_7$] (Zachariasen, 1930) aristotype with two formula units in the space group $C2/m$. A peculiarity of this structure type is a linear As—O—As bridging unit. Like several other compounds with thortveitite-type structures, $Co_2As_2O_7$, $Ni_2As_2O_7$ and $Cu_2As_2O_7$ are dimorphic

[1] In the older literature the synonymous term 'pyroarsenate' is much more common.

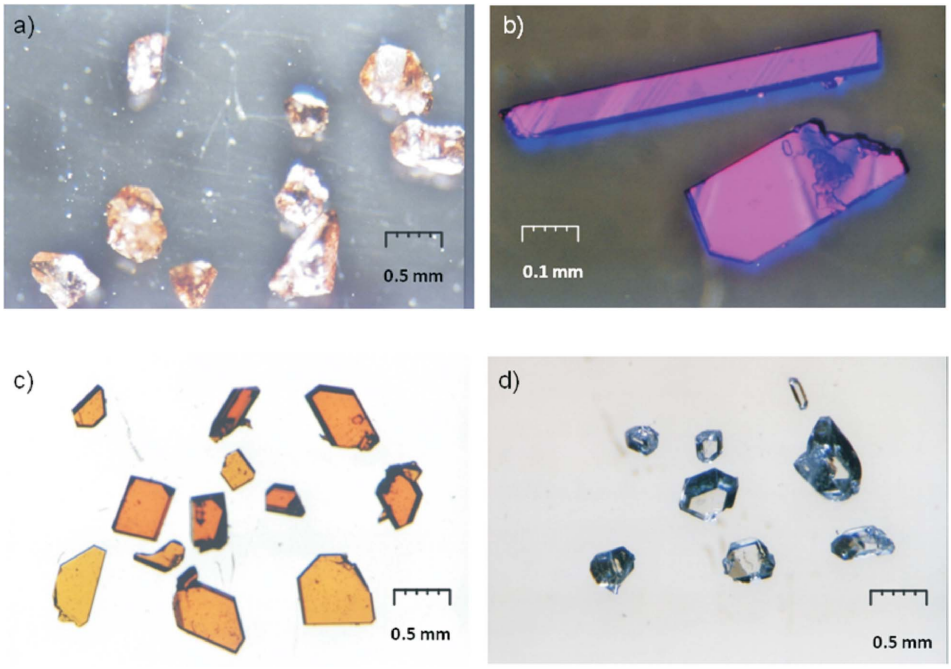

Figure 1
Photographs of the $M_2As_2O_7$ crystals obtained: (*a*) $Mn_2As_2O_7$; (*b*) $Co_2As_2O_7$; (*c*) $Ni_2As_2O_7$; (*d*) $Zn_2As_2O_7$.

and undergo reversible α (low-temperature) $\leftrightarrow$ β (high-temperature) phase transitions (Buckley *et al.*, 1990; Weil *et al.*, 2004*a*,*b*), whereas for the Mg, Cd and Mn diarsenates dimorphism has not been observed. For the sake of completeness it should be noted that $Sr_2As_2O_7$ (Weil *et al.*, 2009) is isotypic with the high-temperature polymorphs (β forms) of $Ca_2P_2O_7$ (Boudin *et al.*, 1993) and $Sr_2V_2O_7$ (Baglio & Dann, 1972), and likewise shows no polymorphism. However, this compound is not structurally related to the aforementioned metal and 3*d* transition metal diarsenates because the ionic radius of Sr^{2+} (Shannon, 1976) is too large to adopt the thortveitite structure type or a variant thereof.

Low-temperature α-$Cu_2As_2O_7$ (Weil *et al.*, 2004*a*) crystallizes isotypically with α-$Cu_2P_2O_7$ (Robertson & Calvo, 1967; Effenberger, 1990) and β-$Cu_2V_2O_7$ (Mercurio-Lavaud & Frit, 1973; Hughes & Brown, 1989) with four formula units in the space group *C*2/*c*. In this structure type the X_2O_7 (X = P, As, V) groups are bent. For the corresponding low-temperature α forms of the Co and Ni diarsenates triclinic unit cells were unambiguously deduced from neutron powder data, but structure refinements under consideration of a relation to the thortveitite structure by reducing the symmetry, *e.g.* by multiplying one or more crystal axes, were unsatisfactory for both phases (Buckley *et al.*, 1990). Although magnetic structures for $Co_2As_2O_7$ and $Ni_2As_2O_7$ were discussed (Buckley *et al.*, 1995), the crystal structures of the low-temperature α phases of $Co_2As_2O_7$ and $Ni_2As_2O_7$ remained unsolved until now. The same applies to $Zn_2As_2O_7$. To our knowledge, results of structural studies of this compound have not been published so far. This motivated us to grow single crystals of $M_2As_2O_7$ diarsenates for structure analysis. A convenient way to obtain high-quality single crystals makes use of chemical transport reactions (Schäfer, 1964). This method has been successfully applied for single-crystal growth of various transition metal phosphates (Glaum, 1999; Gruehn & Glaum, 2000). By analogy, it was shown that this preparative method can likewise be used for single-crystal growth of transition metal arsenates like $Cd_2As_2O_7$ (Weil, 2001), $Cu_2As_2O_7$ (Weil *et al.*, 2004*a*,*b*) or $Fe^{II}_3Fe^{III}_4(AsO_4)_6$ (Weil, 2004).

In this article details of single-crystal growth and the thermal behaviour of the $M_2As_2O_7$ diarsenates (M = Mn, Co, Ni, Zn) are reported. The corresponding crystal structures of $Mn_2As_2O_7$, the low-temperature (α) polymorphs of $Co_2As_2O_7$, $Ni_2As_2O_7$ and $Zn_2As_2O_7$, and of the incommensurately modulated β-$Zn_2As_2O_7$ polymorph are discussed with respect to their relation to the ideal thortveitite structure. For this purpose superspace models are also applied.

2. Experimental

2.1. Preparation

Single crystals of all four $M_2As_2O_7$ diarsenates were grown *via* chemical transport reactions (Schäfer, 1964; Gruehn & Glaum, 2000) in sealed and evacuated silica tubes with an approximate volume of 15 cm^3. Starting from stoichiometric 2:1 mixtures of the component oxides MO and As_2O_5, a temperature gradient of 1153 $\rightarrow$ 1073 K was applied. Chlorine gas was used as the transport agent and was provided by thermolysis of $PtCl_2$ (50 mg) that was also present in the reaction mixture. After a reaction period of 1 week, the one-pot reaction was completed and no solids were left in the source region of the ampoule. The $M_2As_2O_7$ diarsenate crystals grew in the sink region of the ampoule and were removed from the glass wall with diluted hydrofluoric acid (5%$_{wt}$). $Mn_2As_2O_7$ crystals are flesh-coloured, $Co_2As_2O_7$ crystals are pleochroic (purple to dark blue), $Ni_2As_2O_7$ crystals are orange and $Zn_2As_2O_7$ crystals are colourless (Fig. 1).

2.2. Thermal analysis

Differential scanning calorimetry (DSC) measurements of the four diarsenate phases $M_2As_2O_7$ were performed employing a NETZSCH DSC-204 Phoenix® system (temperature range: 233–773 K; aluminium crucible with

Table 1
Details of crystal data and structure refinements of $Mn_2As_2O_7$ and of the α-$M_2As_2O_7$ structures as described in commensurately modulated superstructures.

	$Mn_2As_2O_7$	α-$Co_2As_2O_7$	α-$Ni_2As_2O_7$	α-$Zn_2As_2O_7$
Crystal data				
Chemical formula	$As_2Mn_2O_7$	$As_2Co_2O_7$	$As_2Ni_2O_7$	$As_2Zn_2O_7$
M_r	371.7	379.7	379.2	392.6
Crystal system, space group	Monoclinic, *C*2/*m*	Triclinic, $P\bar{1}$	Triclinic, *P*1	Monoclinic, *I*2/*c*
Temperature (K)	295	295	295	240
a, *b*, *c* (Å)	6.7454 (8), 8.7561 (10), 4.8004 (7)	32.9920 (16), 5.3332 (4), 8.9775 (6)	19.497 (4), 5.297 (1), 8.868 (2)	20.5802 (3), 8.4360 (1), 9.6180 (1)
α, β, γ (°)	90, 102.723 (12), 90	58.472 (1), 149.011 (1), 126.976 (1)	58.32 (2), 148.78 (2), 127.30 (2)	90, 106.5640 (7), 90
V (Å^3)	276.57 (6)	649.64 (9)	377.5 (3)	1600.53 (3)
Z	2	5	3	12
Radiation type	Mo $K\alpha$	Mo $K\alpha$	Mo $K\alpha$	Mo $K\alpha$
μ (mm^{-1})	16.42	19.00	20.51	21.28
Crystal size (mm)	0.29 × 0.29 × 0.14	0.18 × 0.15 × 0.02	0.23 × 0.18 × 0.08	0.18 × 0.12 × 0.02
Data collection				
Diffractometer	Nonius CAD-4	Bruker SMART CCD	Bruker SMART CCD	Bruker APEXII CCD
Absorption correction	Numerical *HABITUS* (Herrendorf, 1997)	Numerical *HABITUS* (Herrendorf, 1997)	Numerical *HABITUS* (Herrendorf, 1997)	Multi-scan *SADABS* (Bruker, 2009)
T_{min}, T_{max}	0.061, 0.222	0.109, 0.590	0.109, 0.554	0.361, 0.749
No. of measured, independent and observed [$I > 3\sigma(I)$] reflections	3857, 1012, 937	7549, 3866, 3229	13 779, 5394, 5331	39 828, 6626, 4899
R_{int}	0.040	0.055	0.067	0.048
Refinement				
$R[F^2 > 2\sigma(F^2)]$, $wR(F^2)$, S	0.037, 0.045, 3.26	0.029, 0.034, 1.63	0.027, 0.032, 1.76	0.023, 0.032, 1.23
No. of reflections	1012	3866	5394	6626
No. of parameters	32	251	297	151
$\Delta\rho_{max}$, $\Delta\rho_{min}$ (e Å^{-3})	3.39, −3.00	1.60, −1.51	1.40, −0.71	1.01, −0.90
Flack parameter	–	–	0.02 (1)	–

Computer programs used: *CAD*-4 (Enraf–Nonius, 1989), *SMART* (Bruker, 2004), *APEX*2 (Bruker, 2009), *SAINT* (Bruker, 2004), *HELENA* implemented in *PLATON* (Spek, 2009), *SHELXS* (Sheldrick, 2008), *JANA*2006 (Petříček *et al.*, 2006), *ATOMS* (Dowty, 2006).

pierced lid; N_2 atmosphere; 20 ml min^{-1}; heating/cooling rate: 10 K min^{-1}). Other than $Mn_2As_2O_7$, all other diarsenates $M_2As_2O_7$ are dimorphic with phase transition points of *ca* 453 (Co), 694 (Ni) and 272 K (Zn). All phase transitions show only slight hystereses (Fig. 2).

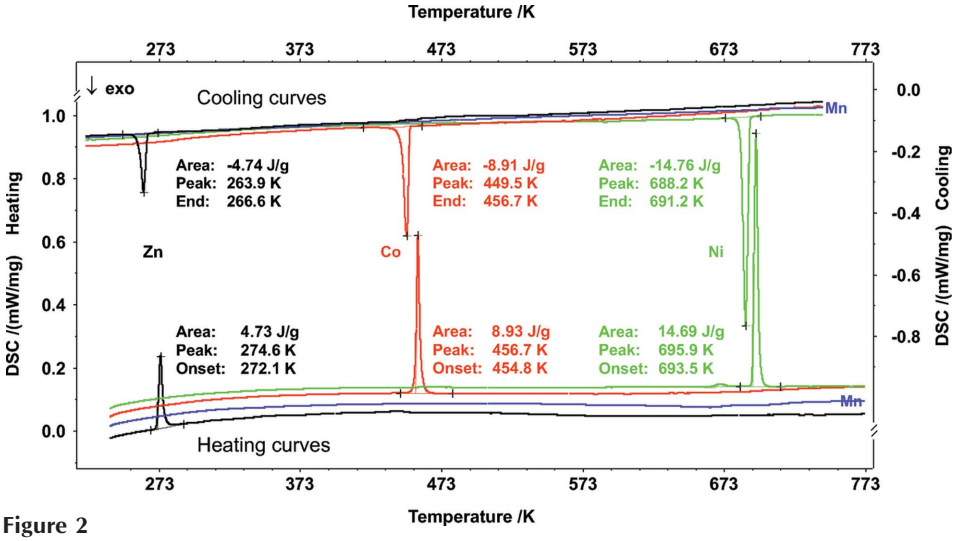

Figure 2
DSC curves (heating and cooling) of the four $M_2As_2O_7$ (M = Mn, Co, Ni, Zn) compounds in the range 233–773 K showing reversible phase transitions for the Co, Ni and Zn phases; the Mn phase shows no phase transition.

2.3. Single-crystal X-ray diffraction

Prior to X-ray data collections, the quality of selected crystals was checked under a polarizing microscope. Whereas $Mn_2As_2O_7$, $Ni_2As_2O_7$ and $Zn_2As_2O_7$ were obtained in single crystalline forms, nearly all $Co_2As_2O_7$ crystals were polysynthetically twinned with a pronounced formation of parallel domains, as depicted in Fig. 1(*b*). A single-domain region was cut out of a large $Co_2As_2O_7$ crystal for subsequent X-ray data collections. For that purpose the selected crystals were mounted on thin silica glass fibres and their quality was tested on a SMART CCD three-circle diffractometer (Bruker AXS) by performing a quick data collection. The crystals with the best performance with respect to diffraction intensities, R_i values and splitting of reflections were eventually used for the final data collections. For all final data collections, performed either using

Table 2
Details of crystal data and structure refinement of incommensurately modulated β-$Zn_2As_2O_7$ and of the commensurately modulated α-$M_2As_2O_7$ structures in the superspace description.

	β-$Zn_2As_2O_7$-superspace	α-$Co_2As_2O_7$-superspace	α-$Ni_2As_2O_7$-superspace	α-$Zn_2As_2O_7$-superspace
Crystal data				
Chemical formula	$As_2O_7Zn_2$	$As_2Co_2O_7$	$As_2Ni_2O_7$	$As_2Zn_2O_7$
M_r	392.6	379.7	379.2	392.6
Crystal system, superspace group	Monoclinic, $C2/m(\alpha,0,\gamma)0s$	Triclinic, $C\bar{1}$ (α,β,γ)	Triclinic, $C1(\alpha,\beta,\gamma)$	Monoclinic, $C2/m(\alpha,0,\gamma)0s$
Temperature (K)	298	298	298	240
t_o	–	0	0	0
q	0.3190 (1), 0, 0.3717 (1)	1/5, 1/5, 1/5	1/3, 1/3, 1/3	−1/3, 0, 0.5
a, b, c (Å)	6.7248 (1), 8.4605 (2), 4.7791 (1)	6.598 (1), 8.523 (1), 4.751 (1)	6.499 (1), 8.427 (3), 4.722 (5)	6.860 (1), 8.4360 (1), 4.8090 (1)
α, β, γ (°)	90, 105.319 (1), 90	89.30 (1), 103.359 (5), 88.771 (3)	89.19 (7), 103.28 (5), 89.46 (3)	90, 106.5640 (7), 90
V (Å^3)	262.216 (3)	259.85 (7)	251.7 (3)	266.756 (5)
Z	2	2	2	2
Radiation type	Mo $K\alpha$	Mo $K\alpha$	Mo $K\alpha$	Mo $K\alpha$
μ (mm^{-1})	21.65	19.00	20.51	21.28
Crystal size (mm^3)	0.12 × 0.10 × 0.05	0.18 × 0.15 × 0.02	0.23 × 0.18 × 0.08	0.18 × 0.12 × 0.02
Data collection				
Diffractometer	Bruker APEXII CCD	Bruker SMART CCD	Bruker SMART CCD	Bruker APEXII CCD
Absorption correction	*SADABS* (Bruker, 2009)	*HABITUS* (Herrendorf, 1997)	*HABITUS* (Herrendorf, 1997)	*SADABS* (Bruker, 2009)
T_{min}, T_{max}	0.212, 0,790	0.109, 0.590	0.109, 0.554	0.361, 0.749
No. of measured reflections	24 775	7549	13 779	39 828
No. of independent main reflections (all/obs)	1764/1486	779/734	1792/1780	1155/1080
No. of independent first-order reflections (all/obs.)	3256/1787	1541/1221	3602/3551	2107/1755
No. of independent second-order reflections (all/obs.)	3519/421	1546/1274	–	2311/1718
No. of independent third-order reflections (all/obs.)	–	–	–	1053/346
Criterion for observed reflections	$I > 3\sigma(I)$	$I > 3\sigma(I)$	$I > 3\sigma(I)$	$I > 3\sigma(I)$
R_{int}	0.042	0.055	0.067	0.048
Refinement				
$R[F^2 > 2\sigma(F^2)]$, $wR(F^2)$, S	0.029, 0.046, 0.92	0.029, 0.034, 1.63	0.027, 0.032, 1.76	0.023, 0.032, 1.24
All reflections	0.029/0.046	0.029/0.034	0.027/0.032	0.023/0.032
Main reflections	0.021/0.030	0.028/0.035	0.029/0.035	0.018/0.026
First-order reflections	0.037/0.045	0.031/0.034	0.025/0.030	0.023/0.027
Second-order reflections	0.094/0.150	0.028/0.033	–	0.030/0.033
Third-order reflections	–	–	–	0.063/0.123
No. of reflections	8539	3866	5394	6626
No. of parameters	135	251	296	149
$\Delta\rho_{max}$, $\Delta\rho_{min}$ (e Å^{-3})	1.22, −1.28	1.61, −1.50	1.40, −0.71	1.04, −0. 94

Computer programs used: see Table 1.

the *SMART* system (Bruker AXS), a Nonius *CAD*-4 system or on an APEXII four-circle diffractometer (Bruker AXS), complete reciprocal spheres with high redundancy were measured. For low-temperature measurements, the crystals were cooled in a stream of nitrogen using an Oxford Cryosystem cooling device. Details of data collections are gathered in Tables 1 and 2.

For $Co_2As_2O_7$, $Ni_2As_2O_7$ and $Mn_2As_2O_7$, numerical absorption corrections were applied using the program *HABITUS* (Herrendorf, 1997). For both $Zn_2As_2O_7$ polymorphs a semi-empirical absorption correction based on the multi-scan approach of *SADABS* (Bruker, 2009) was carried out. Correction for extinction based on the B-C type 1 Lorentzian model (Becker & Coppens, 1974) was carried out using *JANA*2006 (Petříček *et al.*, 2006).

2.4. X-ray powder diffraction

X-ray powder diffraction measurements were performed with Cu $K\alpha_{1,2}$ radiation (1.54060, 1.54439 Å) on a PanAlytical X'Pert Pro diffractometer with Bragg–Brentano geometry equipped with an X'Celerator multi-channel detector with 2.546° scan length. For data recording, the finely ground microcrystalline material was placed on a silicon single-crystal sample holder that was spun with a frequency of eight rotations per minute. Rietveld refinements were performed with *TOPAS* (Version 4.1; Bruker, 2008).

3. Structure solutions and refinements

The unit-cell determination of $Mn_2As_2O_7$ confirmed the *C*-centred cell of the thortveitite structure type as reported in

previous powder studies (Buckley *et al.*, 1990; Aranda *et al.*, 1991). In comparison with the latter, the current refinement of $Mn_2As_2O_7$ based on single-crystal X-ray data led to more accurate results in terms of bond lengths and anisotropic displacement parameters. Since the $Mn_2As_2O_7$ structure represents the aristotype of all other structures reported in this article, we will also deal with this structure in detail.

Unit-cell determination of α-$Co_2As_2O_7$ showed a primitive cell with triclinic symmetry and reduced cell parameters of a = 5.3332 (4), b = 7.6789 (6), c = 16.0428 (12) Å, α = 82.916 (1), β = 88.474 (1), γ = 85.229 (1)°, V = 649.64 (9) Å^3. Structure solution with *SHELXS*97 (Sheldrick, 2008) revealed a thortveitite-related fivefold superstructure in the space group $P\bar{1}$ with a 2.5-fold volume increase.

A 1.5-fold cell volume increase with respect to the thortveitite structure (threefold volume increase with respect to the reduced thortveitite cell) was determined for α-$Ni_2As_2O_7$. Here a threefold superstructure, likewise with triclinic lattice symmetry, was found with reduced lattice parameters of a = 5.297 (1), b = 7.574 (2), c = 10.160 (2) Å, α = 72.87 (3), β = 75.75 (3), γ = 85.15 (3)°, V = 377.51 (14) Å^3. Structure refinements in the centrosymmetric space group $P\bar{1}$ led to unreasonable models with rather high reliability factors. A satisfactory model was only achieved in the space group $P1$. An analysis of the coordinates of the actual atoms showed no apparent higher symmetry, with maximum deviations from an idealized centrosymmetric structure of up to 0.11 Å for As atoms, 0.08 Å for Ni atoms and 0.44 Å for O atoms. Moreover, the refined Flack parameter (Flack, 1983; Flack & Bernardinelli, 1999) of 0.02 (1) gives a clear indication of the absence of a centre of symmetry.

A first cell determination of several β-$Zn_2As_2O_7$ crystals based on room-temperature data indicated a *C*-centred monoclinic cell with lattice parameters close to the ideal thortveitite-type cell of $Mn_2As_2O_7$. However, many weak reflections could not be indexed on the basis of this cell or by increasing the cell volume; subsequent structure refinements of the *C*-centred thortveitite structure model remained unsatisfactory. A careful examination of the diffraction spots in reciprocal space with the program *RLATT* (Bruker, 2004) and of pseudo-precession photographs extracted from CCD images revealed diffraction patterns with main reflections and additional satellite reflections. All these satellite reflections could be indexed with the *SAINT* software (Bruker, 2009) with four integers as $\mathbf{H} = h\mathbf{a}^* + k\mathbf{b}^* + l\mathbf{c}^* + m\mathbf{q}$ with $\mathbf{q}$ = [0.3190 (1), 0, 0.3717 (1)] up to the order $|m| = 2$ (reflections with $|m| = 2$ already very weak). From the observed monoclinic lattice symmetry and the reflection conditions ($hklm$, $h + k = 2n$) and ($h0lm$, $m = 2n$) the superspace groups $Cm(\alpha,0,\gamma)s$ and $C2/m(\alpha, 0,\gamma)0s$ were derived. Subsequent structure refinements with *JANA*2006 (Petříček *et al.*, 2006) confirmed the centrosymmetric superspace group $C2/m(\alpha,0,\gamma)0s$.

Comparison of lattice parameters, superspace group and the $\mathbf{q}$ vector of β-$Zn_2As_2O_7$ with those of the α_2-phase of chromium(II) diphosphate, $Cr_2P_2O_7$ (Palatinus *et al.*, 2006) showed an obvious relation between the two structures. For reasons of consistency, we have taken the atomic coordinates of α_2-$Cr_2P_2O_7$ as starting parameters for refinement of the final structure model of β-$Zn_2As_2O_7$. For the commensurate low-temperature α-$Zn_2As_2O_7$ polymorph the atomic coordinates of the isotypic low-temperature phase α_1-$Cr_2P_2O_7$ (Palatinus *et al.*, 2006) were taken as the starting model for structure refinement.

For the final refinements of the α-$M_2As_2O_7$ (M = Co, Ni, Zn) structures, the unit cells are described with non-standard settings (Table 1). From a practical point of view we have chosen the cells in such a way that the orientation of the structural building blocks, *viz.* alternate layers of diarsenate and metal oxide units, are arranged in a similar fashion as in the thortveitite aristotype structure. For each α-$M_2As_2O_7$ (M = Co, Ni, Zn) structure the layers extend parallel to (001). Moreover, these settings are also comparable with the unit cells of the incommensurately modulated β-$Zn_2As_2O_7$ structure and of the $Cr_2P_2O_7$ polymorphs (Palatinus *et al.*, 2006). Consequently, a close relation of all these structures is obvious.

The relations between the *C*-centred basic cell (subscript b) and the cells of the commensurate superstructures (subscript s) are given by the following relations

$$\alpha\text{-}Co_2As_2O_7 : (\mathbf{a}_s, \mathbf{b}_s, \mathbf{c}_s) = (\mathbf{a}_b, \mathbf{b}_b, \mathbf{c}_b)\begin{pmatrix} 5 & -1/2 & -1 \\ 0 & 1/2 & 0 \\ 0 & 0 & 1 \end{pmatrix}; \quad \det(\boldsymbol{P}) = 2.5 \tag{1}$$

$$\alpha\text{-}Ni_2As_2O_7 : (\mathbf{a}_s, \mathbf{b}_s, \mathbf{c}_s) = (\mathbf{a}_b, \mathbf{b}_b, \mathbf{c}_b)\begin{pmatrix} 3 & -1/2 & -1 \\ 0 & 1/2 & 0 \\ 0 & 0 & 1 \end{pmatrix}; \quad \det(\boldsymbol{P}) = 1.5 \tag{2}$$

$$\alpha\text{-}Zn_2As_2O_7 : (\mathbf{a}_s, \mathbf{b}_s, \mathbf{c}_s) = (\mathbf{a}_b, \mathbf{b}_b, \mathbf{c}_b)\begin{pmatrix} 3 & 0 & 0 \\ 0 & 1 & 0 \\ 0 & 0 & 2 \end{pmatrix}; \quad \det(\boldsymbol{P}) = 6 \tag{3}$$

3.1. Structure refinement of incommensurately modulated $Zn_2As_2O_7$

Refinement of the basic structure of incommensurately modulated β-$Zn_2As_2O_7$, starting with the coordinates of the α_2-$Cr_2P_2O_7$ phase, led to a reasonable model. Since the strategies for refinement of the different chromium(II) diphosphate structures were discussed in detail by Palatinus *et al.* (2006),[2] we will concentrate on the common features and main differences between the β-$Zn_2As_2O_7$ and α_2-$Cr_2P_2O_7$ structures in the following.

[2] Another structure model based on the maximum entropy method (MEM) for the incommensurately modulated α_2-$Cr_2P_2O_7$ structure has recently been published by Li *et al.* (2010). The two models are very similar and differ mainly in the treatment of the disordered P_2O_7 group.

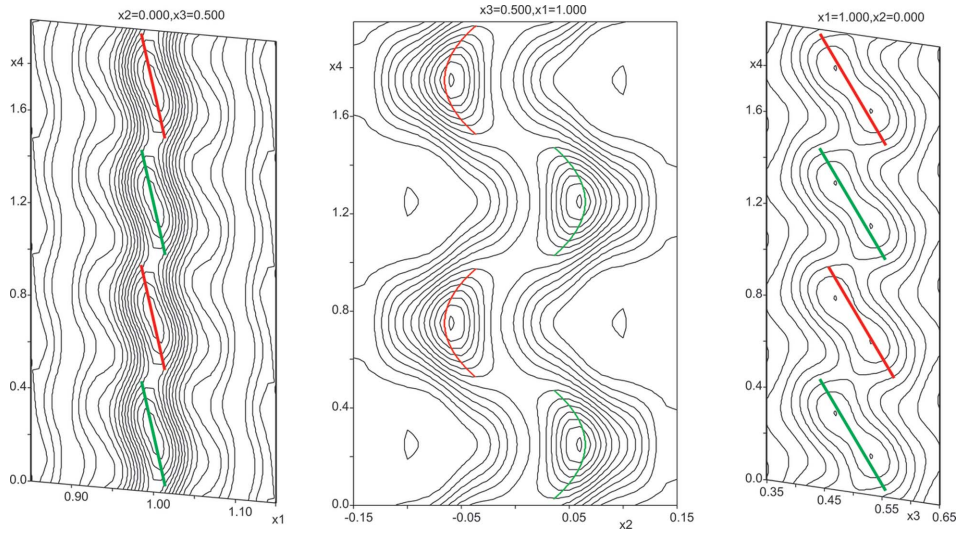

Figure 3
x_n–x_4 sections through the superspace electron density at the position of the O2 atom. Red lines represent the O2 atom, green lines represent O2 atoms created with the symmetry operator $(x_1, -x_2, x_3, x_4 + \frac{1}{2})$. The electron density was summed up over a range of 3 Å in the non-plotted directions. This figure is in colour in the electronic version of this paper.

After refining the atomic coordinates of the basic structure of β-$Zn_2As_2O_7$, positional and ADP modulation waves were carefully added for further refinement steps. The Fourier map of the O2 atom (the As—O—As bridging atom) clearly showed a discontinuity at $x_4 = 0.5$. This atom was subsequently moved from Wyckoff position 2*c* (site symmetry 2/*m*) towards position 4*h* (site symmetry 2). Its occupational modulation was described by a crenel function in the range x_4 = [0,0.5]. For x_4 = [0.5,1] the symmetry operator $(x_1, -x_2, x_3, x_4 + \frac{1}{2})$ generates a complementary counterpart of O2. Since the x_2 coordinate of the modulation vector is zero, for every value of t either O2 or its counterpart exhibit full occupancy (Fig. 3). The displacive modulation and modulation of ADPs of O2 were modelled using a set of Legendre polynomials $P_i(x)$ of degree $i \geq 1$ with domain of definition $x \in [-1,1]$ instead of harmonic functions. The polynomials are scaled onto the non-zero part of the crenel function. Legendre polynomials of the order $i = 2m$ ($m \in$ N) are even, those of the order $i = 2m + 1$ ($m \in$ N) are odd. Therefore, symmetry operations which leave the crenel function unchanged impose symmetry restrictions analogous to the case of harmonic modulation functions. All Legendre polynomials are pairwise orthogonal on the domain of definition $x \in [-1,1]$, thus no special orthogonalized sets of functions have to be used to avoid correlation of parameters as in the case of harmonic modulation functions (Petříček *et al.*, 1995). Furthermore, it has been empirically shown that small sets of Legendre polynomials are well suited for the description of modulation functions in actual structures (Petříček & Dušek, 2010). The displacive modulation of the O2 atom was modelled only with Legendre polynomials up to the second degree. Thus, the positions of the O2 atom are located on parabolic segments in superspace.

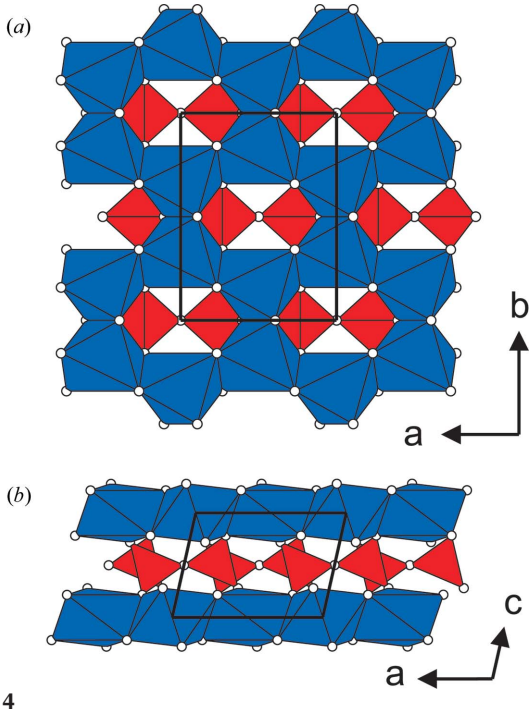

Figure 4
Projection of the thortveitite-type $Mn_2As_2O_7$ structure onto the (001) plane (*a*) and the (010) plane (*b*). MnO_6 octahedra are given in blue, AsO_4 tetrahedra are red. This figure is in colour in the electronic version of this paper.

The Fourier maps of the Zn atom and of O3 (terminal O atom of the AsO_4 tetrahedron) clearly displayed a sawtooth-like modulation. These atoms were also modelled with Legendre polynomials. No additional sawtooth function was introduced because the first-degree Legendre polynomial $P_1(x) = x$ already corresponds to a sawtooth function. For the O3 atom, the point of discontinuity was constrained to the same t position as for O2 to obtain an AsO_4 tetrahedron with reasonable bond lengths and angles for all values of t. The position of the point of discontinuity of the Zn atom in the β-$Zn_2As_2O_7$ structure is independent from the points of discontinuity of the coordinating O atoms. Nevertheless, the bond lengths and angles of the ZnO_x polyhedra are reasonable and no suspicious electron densities in the difference Fourier maps are found.

In the final refinement cycles only modulation functions with non-negligible amplitudes and a significant influence on R factors were retained. In summary, harmonic modulation functions were used for the Zn, As and O1 atoms (for each 2× displacive, 2× ADP), and Legendre polynomials were applied

Table 3
Selected interatomic distances (Å) and angles (°) in the $M_2As_2O_7$ structures.

$Mn_2As_2O_7$					
Mn—O3^{i}	2.1259 (18)	As—O1	1.666 (2)	As—O2—As^{ii}	180
Mn—O3^{iii}	2.1259 (18)	As—O3	1.6663 (18)		
Mn—O1	2.1765 (14)	As—O3^{iv}	1.6663 (18)		
Mn—O1^{v}	2.1765 (14)	As—O2	1.6949 (3)		
Mn—O3^{vi}	2.290 (2)				
Mn—O3^{vii}	2.290 (2)				

Symmetry codes: (i) $x-\frac{1}{2}, y+\frac{1}{2}, z-1$; (ii) $-x+2, y, -z+1$; (iii) $-x+\frac{3}{2}, y+\frac{1}{2}, -z+1$; (iv) $x, -y, z$; (v) $-x+1, y, -z$; (vi) $-x+1, -y, -z+1$; (vii) $x, -y, z-1$.

α-$Co_2As_2O_7$					
Co-1—O3-5^{i}	2.048 (5)	Co-4—O3-2^{i}	1.983 (3)	As-1—O3-2^{ii}	1.614 (3)
Co-1—O3b-2^{iii}	2.074 (4)	Co-4—O1-2^{iv}	2.087 (3)	As-1—O3b-5^{v}	1.668 (4)
Co-1—O1-5^{iv}	2.093 (3)	Co-4—O3b-5	2.098 (7)	As-1—O1-1	1.679 (3)
Co-1—O1-1	2.130 (2)	Co-4—O3b-4^{i}	2.111 (3)	As-1—O2-1	1.750 (7)
Co-1—O3-1	2.192 (7)	Co-4—O3-4	2.126 (7)	As-2—O3b-4^{v}	1.662 (3)
Co-1—O3b-2	2.196 (7)	Co-4—O1-4	2.143 (2)	As-2—O3-3^{ii}	1.667 (3)
Co-2—O3b-1^{iii}	2.052 (3)	Co-5—O3-1^{i}	2.015 (5)	As-2—O1-2	1.674 (3)
Co-2—O3b-3	2.084 (7)	Co-5—O1-1^{iv}	2.031 (3)	As-2—O2-2	1.6868 (10)
Co-2—O1-4^{iv}	2.090 (3)	Co-5—O1-5	2.113 (2)	As-3—O1-3	1.676 (2)
Co-2—O3-4^{i}	2.105 (6)	Co-5—O3b-3^{i}	2.160 (3)	As-3—O3b-3^{v}	1.673 (3)
Co-2—O1-2	2.121 (2)	Co-5—O3b-1^{vi}	2.177 (7)	As-3—O3-4^{ii}	1.693 (3)
Co-2—O2-1^{vii}	2.406 (3)	Co-5—O3-5	2.310 (7)	As-3—O2-1^{v}	1.745 (7)
Co-3—O3b-5^{i}	2.054 (4)			As-4—O3-5^{ii}	1.666 (3)
Co-3—O3-3^{i}	2.072 (5)			As-4—O3b-2^{v}	1.670 (3)
Co-3—O1-3	2.093 (2)			As-4—O1-4	1.682 (3)
Co-3—O1-3^{iv}	2.142 (3)			As-4—O2-4	1.726 (9)
Co-3—O3-3	2.179 (7)			As-5—O1-5	1.663 (2)
Co-3—O3b-4	2.193 (7)			As-5—O3b-1^{v}	1.674 (4)
				As-5—O3-1^{viii}	1.677 (3)
				As-5—O2-4^{ix}	1.705 (9)
				ØAs—O$_{terminal}$	1.669
				ØAs—O$_{bridging}$	1.723
				As-1—O2-1—As-3^{v}	133.15 (17)
				As-2—O2-2—As-2^{v}	180
				As-4—O2-4—As-5^{ix}	156.43 (16)

Symmetry codes: (i) $-x+1, -y-1, -z$; (ii) $x, y, z+1$; (iii) $-x, -y-1, -z$; (iv) $-x+1, -y, -z$; (v) $-x+1, -y, -z+1$; (vi) $x+1, y, z$; (vii) $x, y-1, z$; (viii) $x+1, y, z+1$; (ix) $-x+2, -y, -z+1$.

α-$Ni_2As_2O_7$					
Nia-1—O3c-2^{vi}	2.021 (3)	Nib-1—O3a-1	1.967 (3)	Asa-1—O3a-3	1.658 (3)
Nia-1—O3d-1	2.051 (7)	Nib-1—O3b-1^{ix}	2.056 (7)	Asa-1—O3c-3^{i}	1.665 (3)
Nia-1—O1a-1	2.084 (2)	Nib-1—O3c-1	2.064 (7)	Asa-1—O2-1	1.694 (8)
Nia-1—O1b-1^{v}	2.105 (3)	Nib-1—O1b-1^{iii}	2.087 (2)	Asa-1—O1a-1	1.695 (3)
Nia-1—O3b-1	2.131 (6)	Nib-1—O3d-3^{ix}	2.090 (3)	Asa-2—O3a-1^{iii}	1.618 (4)
Nia-1—O2-2	2.170 (3)	Nib-1—O1a-1^{viii}	2.115 (3)	Asa-2—O3c-1	1.675 (4)
Nia-2—O1b-2^{v}	2.049 (3)	Nib-2—O3a-2^{v}	2.010 (5)	Asa-2—O1a-2^{ii}	1.690 (3)
Nia-2—O3c-3^{v}	2.052 (4)	Nib-2—O1a-2^{iii}	2.011 (3)	Asa-2—O2-2	1.757 (6)
Nia-2—O3b-2	2.054 (5)	Nib-2—O1b-2^{x}	2.051 (2)	Asa-3—O1a-3	1.673 (2)
Nia-2—O1a-2	2.070 (2)	Nib-2—O3d-1^{iv}	2.116 (3)	Asa-3—O3c-2^{i}	1.673 (4)
Nia-2—O3a-2^{v}	2.116 (7)	Nib-2—O3b-2	2.157 (7)	Asa-3—O3a-2	1.680 (3)
Nia-2—O3d-2	2.162 (7)	Nib-2—O3c-2^{v}	2.210 (7)	Asa-3—O2-3	1.690 (8)
Nia-3—O3c-1^{v}	2.026 (3)	Nib-3—O1a-3^{iii}	2.020 (3)	Asb-1—O3b-2^{i}	1.675 (3)
Nia-3—O1a-3	2.048 (2)	Nib-3—O3a-3^{v}	2.026 (5)	Asb-1—O3d-2	1.680 (3)
Nia-3—O3b-3	2.076 (5)	Nib-3—O3d-2	2.041 (4)	Asb-1—O1b-1^{iv}	1.682 (3)
Nia-3—O3d-3	2.122 (7)	Nib-3—O1b-3^{v}	2.049 (2)	Asb-1—O2-3	1.726 (8)
Nia-3—O1b-3^{vii}	2.144 (3)	Nib-3—O3b-3	2.124 (7)	Asb-2—O1b-2	1.671 (2)
Nia-3—O3a-3^{v}	2.192 (7)	Nib-3—O3c-3^{v}	2.228 (7)	Asb-2—O3b-3^{i}	1.671 (3)
				Asb-2—O3d-3	1.677 (4)
				Asb-2—O2-1	1.712 (8)
				Asb-3—O3d-1^{iii}	1.680 (2)
				Asb-3—O1b-3	1.693 (2)
				Asb-3—O3b-1	1.709 (3)
				Asb-3—O2-2	1.779 (7)
				ØAs—O$_{terminal}$	1.676
				ØAs—O$_{bridging}$	1.726
				Asa-1—O2-1—Asb-2	152.34 (14)
				Asa-2—O2-2—Asb-3	126.10 (16)
				Asa-3—O2-3—Asb-1	157.74 (15)

for Zn (6× positional coefficients, 4× ADP) for O2 (2× positional, 2× ADP) and O3 (4× positional, 4× ADP) atoms.

Regarding the number of refinable parameters, a pair of two Legendre polynomials $P_{(2n+1)}(x)$ and $P_{(2n+2)}(x)$ corresponds to one harmonic wave. While it is well understood that the maximum harmonic generally must be less than or equal to the maximum order of satellite reflections, the situation for Legendre polynomials is not as clear and has to be carefully evaluated for each modulation function. Indeed, although only satellites up to order $|m| = 2$ were observed, increasing the number of Legendre polynomials used in the refinement of the displacive modulation of the Zn atom from 4 to 6 resulted in significantly better R values, in particular for the main reflections and distinctly less difference electron density in the difference Fourier maps. Further increase in the number of Legendre polynomials had negligible effect on the R values and resulted in an unreasonable shape of the modulation function close to the point of discontinuity.

3.2. Superspace models of the commensurate structures

For refinements of the commensurate α modifications of the $M_2As_2O_7$ (M = Co, Ni, Zn) structures we have alternatively used the superspace approach (van Smaalen, 1995) based on the ideal thortveitite structure of $Mn_2As_2O_7$. The usefulness of such a description for polymorphic structures with a (common) superspace model was already shown for the related structures of the various $Cr_2P_2O_7$ phases, and the low-temperature modifications of other $M_2P_2O_7$ diphosphates (Palatinus *et al.*, 2006) that all crystallize in the ideal thortveitite structure type with their high-temperature modifications.

For the three α-$M_2As_2O_7$ structures described here, only α-$Zn_2As_2O_7$ can be directly derived from the monoclinic thortveitite basic structure using the same superspace group $C2/m(\alpha,0,\gamma)0s$ and the **q** vector $[-\frac{1}{3}, 0, \frac{1}{2}]$. Since α-$Zn_2As_2O_7$ is isotypic with the low-temperature structures of α_1-$Cr_2P_2O_7$ (Palatinus *et al.*, 2006) and α-$Zn_2P_2O_7$ (Robertson & Calvo, 1970), we have taken the atomic coordinates of the chromium phase as a starting model for refinement. The structures of α-$Co_2As_2O_7$ and α-$Ni_2As_2O_7$ belong to the triclinic crystal

Table 3 (continued)

Symmetry codes: (i) $x+1, y, z+1$; (ii) $x, y, z-1$; (iii) $x, y-1, z$; (iv) $x, y, z+1$; (v) $x, y+1, z$; (vi) $x, y+1, z-1$; (vii) $x+1, y+1, z$; (viii) $x, y+1, z+1$; (ix) $x-1, y, z$; (x) $x, y-1, z+1$.

α-$Zn_2As_2O_7$ (commensurate structure)					
Zn-1—O3-5^{i}	1.9405 (12)	Zn-3—O3-2^{ii}	2.0406 (10)	As-1—O3-1	1.6683 (11)
Zn-1—O3-1^{iii}	2.0183 (10)	Zn-3—O1-3	2.0683 (11)	As-1—O1-1	1.6707 (10)
Zn-1—O1-1	2.0502 (11)	Zn-3—O3-4^{iv}	2.0897 (10)	As-1—O3-4^{v}	1.6729 (11)
Zn-1—O1-3^{vi}	2.0655 (10)	Zn-3—O1-1^{vi}	2.1006 (11)	As-1—O2-1	1.7146 (13)
Zn-1—O3-4^{vii}	2.0990 (13)	Zn-3—O3-6^{vii}	2.1443 (13)	As-2—O3-5^{v}	1.6429 (12)
Zn-2—O3-3^{ii}	1.9646 (12)	Zn-3—O3-1	2.1977 (13)	As-2—O3-2	1.6718 (12)
Zn-2—O3-6^{i}	2.0272 (11)			As-2—O1-2	1.6790 (10)
Zn-2—O1-2^{vi}	2.0609 (11)			As-2—O2-1^{viii}	1.7338 (14)
Zn-2—O3-2^{viii}	2.0693 (13)			As-3—O3-3^{ix}	1.6506 (12)
Zn-2—O1-2	2.0828 (10)			As-3—O3-6	1.6731 (12)
				As-3—O1-3^{ix}	1.6761 (10)
				As-3—O2-2	1.7354 (6)
				ØAs—O$_{terminal}$	1.667
				ØAs—O$_{bridging}$	1.728
				As-1—O2-1—As-2^{viii}	146.94 (9)
				As-3—O2-2—As-3^{x}	140.28 (11)

Symmetry codes: (i) $x-\frac{1}{2}, -y-\frac{1}{2}, z-1$; (ii) $-x+\frac{3}{2}, -y-\frac{1}{2}, -z+\frac{1}{2}$; (iii) $-x+\frac{1}{2}, -y-\frac{1}{2}, -z+\frac{1}{2}$; (iv) $x+\frac{1}{2}, -y-\frac{1}{2}, z-1$; (v) $x, -y, z-\frac{1}{2}$; (vi) $-x+1, -y, -z$; (vii) $x, y, z-1$; (viii) $-x+1, y, -z+\frac{1}{2}$; (ix) $x, -y, z+\frac{1}{2}$; (x) $-x+2, y, -z+\frac{3}{2}$.

	Average	Minimum	Maximum
β-$Zn_2As_2O_7$ (incommensurate structure)			
Zn-1—O1^{i}	2.079 (2)	2.033 (2)	2.1216 (19)
Zn-1—O3^{ii}	2.020 (4)	1.929 (5)	2.119 (4)
Zn-1—O3^{iii}	2.361 (5)	2.126 (5)	2.800 (5)
As—O1	1.6725 (14)	1.6689 (14)	1.6768 (14)
As—O2	1.723 (2)	1.6769 (10)	1.7735 (13)
As—O3	1.661 (4)	1.636 (4)	1.687 (4)
As—O2—As^{iv}	150.7 (2)	149.18 (16)	152.9 (3)

Symmetry codes: (i) $-x_1+1, x_2, -x_3, -x_4+\frac{1}{2}$; (ii) $x_1-\frac{1}{2}, x_2+\frac{1}{2}, x_3, x_4$; (iii) $-x_1+1, -x_2, -x_3+1, -x_4$; (iv) $-x_1+2, x_2, -x_3+1, -x_4+\frac{1}{2}$; (v) $-x_1+2, -x_2, -x_3+1, -x_4$.

system and hence cannot be derived from a monoclinic superspace group. These commensurate five- (Co) and threefold (Ni) superstructures were refined in superspace groups $C\bar{1}$ (α, β, γ) with $\mathbf{q} = [\frac{1}{5}, \frac{1}{5}, \frac{1}{5}]$ for the Co phase and $C1$(α, β, γ) with $\mathbf{q} = [\frac{1}{3}, \frac{1}{3}, \frac{1}{3}]$ for the Ni phase. According to the descent in symmetry from monoclinic to triclinic, the original five atoms of the $C2/m(\alpha,0,\gamma)0s$ model, *viz.* one *M*, one As and three O atoms, are split into one Co, one As and four O atoms for the α-$Co_2As_2O_7$ model in $C\bar{1}$ (α, β, γ), and into two Ni, two As and six O atoms for the α-$Ni_2As_2O_7$ model in $C1$(α, β, γ). For all superspace models, the labelling of atoms was chosen so that a relation to the basic structure is obvious, *e.g.* an atom related to the O3 atom of the monoclinic thortveitite basic structure becomes atom O3*b* *etc.*

It should be noted that the number of independent parameters in the superspace refinement must not exceed the number of refinable parameters in the supercell description (Palatinus *et al.*, 2006). For the final superspace refinement of the commensurate α_1-$Cr_2P_2O_7$ structure, which is isotypic with α-$Zn_2As_2O_7$, Palatinus *et al.* (2006) eliminated insignificant modulation waves for ADP parameters of some atoms, which lowered the number of refined parameters from 115 to 105. Since our main objective was not an optimization of the refinement strategies of the superspace models, but primarily lies in an equivalent description using both supercell and superspace approaches, we have used the same or only slightly fewer refinement parameters as in the corresponding supercell models. Details of the refinements using the superspace approach are gathered in Table 2.

Full details of all refined structures are given in the supplementary material.[3]

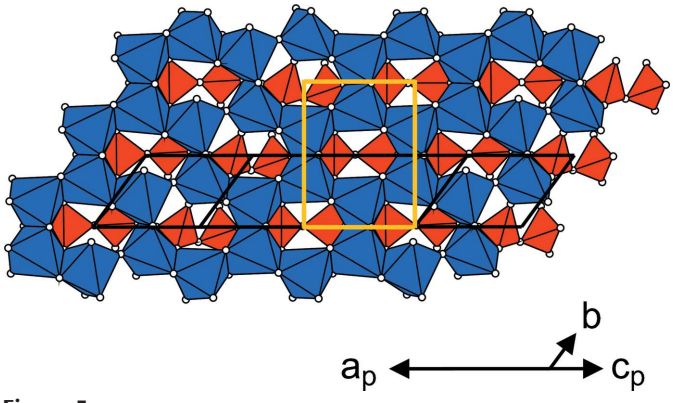

Figure 5
Projection of the α-$Ni_2As_2O_7$ structure along $[\bar{1}0\bar{3}]$. NiO_6 octahedra are given in blue, AsO_4 tetrahedra are red. For clarity only one layer is shown. The unit cell of the thortveitite-type basis structure is indicated with yellow lines. This figure is in colour in the electronic version of this paper.

4. Discussion

The ideal thortveitite-type $Mn_2As_2O_7$ structure is the aristotype of the other arsenates α-$Co_2As_2O_7$, α-$Ni_2As_2O_7$ and α-, β-$Zn_2As_2O_7$. The asymmetric unit of the $Mn_2As_2O_7$ structure contains five atoms, namely one Mn atom, one As atom and three O atoms. For the description of the thortveitite [$Sc_2Si_2O_7$] structure (Zachariasen, 1930) and most of its isotypic $M_2X_2O_7$ congeners the coordinates of the bridging O atom of the X_2O_7 group were chosen to coincide with the origin (Wyckoff position 2*a* with site symmetry 2/*m*). The *M* atom is on position 4*h* (2), the *X* atom on 4*i* (*m*), and the two remaining O atoms are on positions 4*i* (2) and 8*j* (1), respec-

[3] Supplementary data for this paper are available from the IUCr electronic archives (Reference: SN5100). Services for accessing these data are described at the back of the journal.

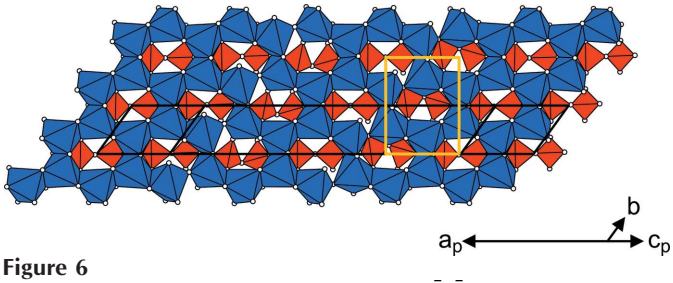

Figure 6
Projection of the α-$Co_2As_2O_7$ structure along $[\bar{1}0\bar{5}]$. CoO_6 octahedra are given in blue, AsO_4 tetrahedra are red. For clarity only one layer is shown. The unit cell of the thortveitite-type basis structure is indicated with yellow lines. This figure is in colour in the electronic version of this paper.

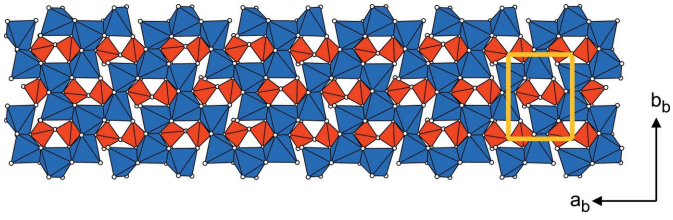

Figure 7
Projection of the incommensurate β-$Zn_2As_2O_7$ structure onto the (001) plane. Only one layer is shown. ZnO_x octahedra are given in blue, AsO_4 tetrahedra are red. The unit cell of the thortveitite-type basis structure is indicated with yellow lines. This figure is in colour in the electronic version of this paper.

tively. For the present refinement of the diarsenate phases, an origin shift along *c*/2 was applied with respect to the original thortveitite cell. This setting is consistent with the description chosen by Palatinus *et al.* (2006), where the *M* atom and the bridging O atom are situated on positions 4*g* and 2*c*, respectively.

The main structural features of the $Mn_2As_2O_7$ aristotype structure are distorted MnO_6 octahedra and As_2O_7 groups with a staggered conformation consisting of two corner-sharing AsO_4 tetrahedra. The MnO_6 octahedra share edges and form two-dimensionally infinite honeycomb sheets extending parallel to (001). The As_2O_7 groups are situated below and above the vacant sites of the cationic layers (Fig. 4). They exhibit a linear As—O—As bridging angle[4] and a large displacement parameter of the bridging O atom perpendicular to the As—O—As axis is observed. In agreement with other X_2O_7 groups consisting of condensed corner-sharing tetrahedral XO_4 units, the *X*—O bond lengths of the bridging O atoms are considerably longer than those of the terminal O atoms (Table 3).

In the different $M_2As_2O_7$ structures (*M* = Co, Ni, Zn) the thortveitite-type basis structure is clearly discernible, but a distinct trend with regard to a change of the coordination numbers of the metal ions from 6 to 5 is obvious. In the ideal thortveitite structure of $Mn_2As_2O_7$ the coordination number of the unique Mn^{2+} ion is 6, with Mn—O bond lengths ranging from 2.1259 (18) to 2.290 (2) Å. Coordination numbers of 6 are also realised for all six crystallographically different Ni^{2+} ions in the α-$Ni_2As_2O_7$ structure (Fig. 5), with a spread of the Ni—O bond lengths from 1.967 (3) to 2.228 (7) Å, accompanied by a distorted octahedral coordination. Three of the five independent Co^{2+} ions in α-$Co_2As_2O_7$ are likewise octahedrally coordinated [1.983 (3)–2.193 (2) Å], whereas the

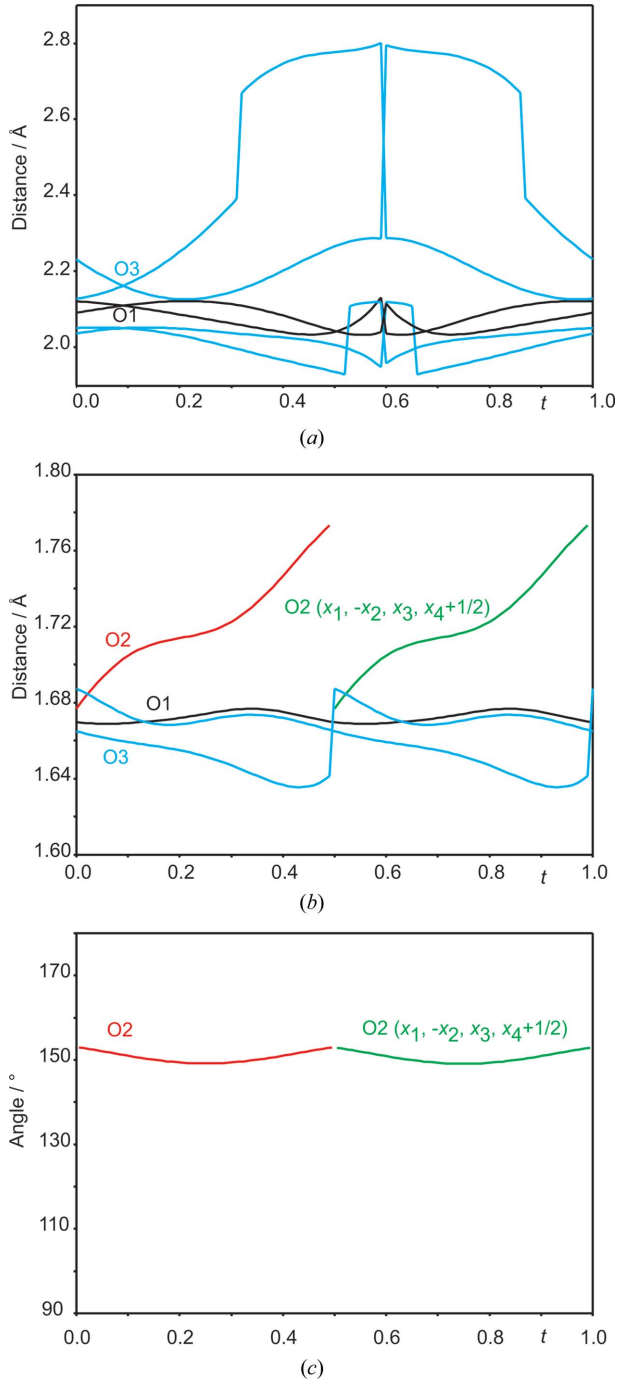

Figure 8
Selected distance and angles range in the incommensurate β-$Zn_2As_2O_7$ structure. (*a*) Zn—O distances, (*b*) As—O distances, (*c*) As—O—As angles.

[4] For the ideal $M_2X_2O_7$ thortveitite structure, a so-called 'split-atom' model was alternatively discussed for the example of $Mn_2P_2O_7$ (Stefanidis & Nord, 1984). In this model the equally disordered bridging O atom is shifted from the centre of symmetry towards a twofold axis (Wyckoff position 4*g*), resulting in a bent *X*—O—*X* angle.

remaining two Co^{2+} ions (Co2 and Co5) have one significantly longer Co—O bond > 2.3 Å and hence may be described as [5 + 1]-coordinate (Fig. 6). As can be seen from Figs. 7 and 8, in the incommensurate β-$Zn_2As_2O_7$ structure the Zn^{2+} ion shows a distinct modulation of its coordination number between 5 and 6. Finally, for the commensurate α-$Zn_2As_2O_7$ structure, two (Zn1 and Zn2) of the three Zn^{2+} ions are clearly five-coordinate [1.9405 (12)–2.0990 (13) Å], with the next-nearest O atom at distances > 3.19 Å, leading to a distorted coordination intermediate between a square pyramid and a trigonal bipyramid. The third Zn^{2+} ion again exhibits coordination number 6 with a distorted octahedral environment and a bond-length distribution between 2.0406 (10) and 2.1977 (13) Å (Fig. 9). An overview with respect to the relations between the individual $M_2As_2O_7$ structures is given in Fig. 10.

Another characteristic distinction between the $Mn_2As_2O_7$ aristotype and the low-temperature α-$M_2As_2O_7$ (M = Co, Ni, Zn) polymorphs pertains to a change from a linear to a bent As—O—As bridging angle. A linear bridging unit is observed only for one As_2O_7 group (As-2) in α-$Co_2As_2O_7$ with the corresponding O2-2 bridging atom likewise located on an inversion centre, whereas the bridging angles of the other two As_2O_7 groups are bent with 133 and 156°. In analogy with the aristotype structure, the bridging O2-2 atom exhibits a high displacement parameter perpendicular to the As—O—As axis. In α-$Ni_2As_2O_7$ and α-$Zn_2As_2O_7$ all As—O—As bridging units clearly deviate from linearity with As—O—As angles of 152, 126, 158° and 147, 140°, respectively. With only a slight modulation between 149 and 153° the preference for the bent As_2O_7 groups can also be seen in the incommensurate β-$Zn_2As_2O_7$ structure (Fig. 8). Irrespective of the linear or bent character of the diarsenate anion in the various $M_2As_2O_7$ (M = Co, Mn, Ni, Zn) structures, the averaged values of the As—$O_{bridging}$ bond lengths are always greater than the corresponding values of the As—$O_{terminal}$ bond lengths, a factor that is observed for most X_2O_7 groups consisting of condensed XO_4 tetrahedra. Selected bond lengths and angles are given in Table 3. The average bond lengths of the AsO_4 groups of 1.669 Å for $Mn_2As_2O_7$, of 1.683 Å for α-$Co_2As_2O_7$, of 1.689 Å for α-$Ni_2As_2O_7$, of 1.682 Å for α-$Zn_2As_2O_7$ and of 1.679 Å for β-$Zn_2As_2O_7$ show only a marginal variation and are in very good agreement with the value of 1.686 Å calculated for more than 700 AsO_4 tetrahedra in various inorganic arsenates(V) (Schwendtner, 2008).

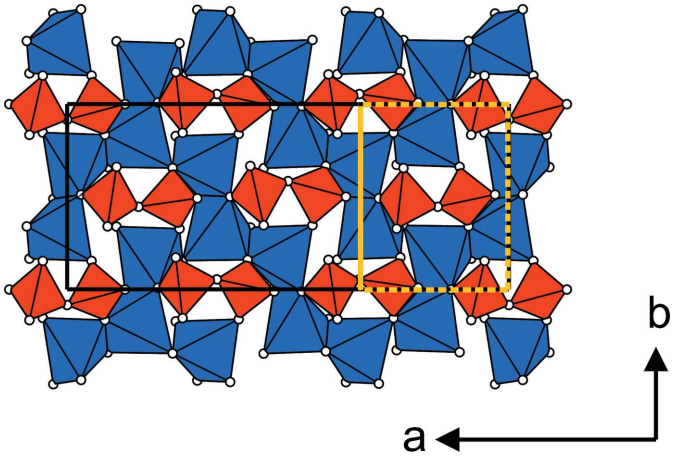

Figure 9
Projection of the commensurate α-$Zn_2As_2O_7$ structure onto (001). ZnO_x octahedra are given in blue, AsO_4 tetrahedra are red. The unit cell of the thortveitite-type basis structure is indicated with (partial) yellow lines. This figure is in colour in the electronic version of this paper.

4.1. Origin of the modulation and comparison with α_2-$Cr_2P_2O_7$

Besides α_2-$Cr_2P_2O_7$, β-$Zn_2As_2O_7$ is the only phase within the $M_2X_2O_7$ family of compounds exhibiting an incommensurately modulated structure. The basic structures of α_2-$Cr_2P_2O_7$ and β-$Zn_2As_2O_7$ can be considered as configurational homeotypic (Bergerhoff *et al.*, 1999). Although they have the same superspace group symmetry and exhibit similar coordinations of the constituents, they differ in the Wyckoff sequence and show clear differences with respect to their modulations. Whereas the diffraction pattern of the Zn phase has discernible satellites only up to the order $|m| = 2$, satellite reflections up to the order $|m| = 4$ were observed for the Cr phase. Moreover, the modulation vector **q** is distinctly different for the two structures, *viz.* **q** = [0.3190 (1), 0, 0.3717 (1)] for β-$Zn_2As_2O_7$ *versus* **q** = [−0.361, 0, 0.471] for α_2-$Cr_2P_2O_7$. The modulation functions of the As atom in β-$Zn_2As_2O_7$ (site symmetry m) exhibit no point of discontinuity, in contrast to the P atom in α_2-$Cr_2P_2O_7$ for which crenel functions and a disorder model were introduced for this atom

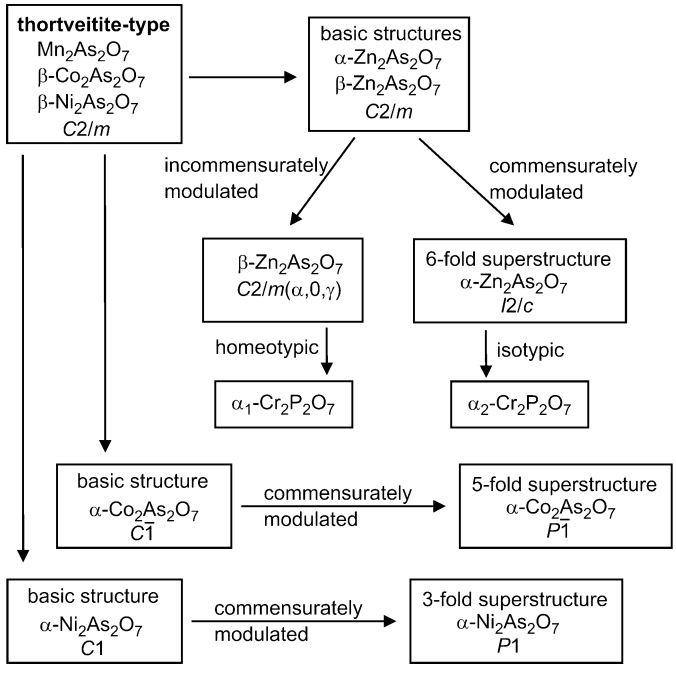

Figure 10
Relationships between the $M_2As_2O_7$ structures, including the $Cr_2P_2O_7$ structures.

and the entire P_2O_7 group. Another main difference between the chromium and the zinc phase pertains to the X—O—X (X = As, P) bridging angles and the corresponding X—O2 distances (neglecting the disorder in the α_2-$Cr_2P_2O_7$ structure). Whereas the P—O2—P angles show a modulation between 146 (4) and 155(3)° with more or less constant P—O2 bond lengths [minimum 1.60 (6) Å, maximum 1.61 (5) Å; Palatinus *et al.*, 2006], the situation in the zinc phase is reversed. Here the As—O2—As angles are only slightly modulated around 150° [min. 149.18 (16)°; max. 152.9 (3)°], but the As—O2 bond lengths vary markedly between 1.6784 (10) and 1.7745 (13) Å (Table 3; Fig. 8). In comparison with phosphorus, the arsenic atom seems to be able to form considerably longer X—O bonds than expected from the mean values for tetrahedral XO_4 groups. Such longer X—O bonds are known from octahedrally coordinated arsenic in various oxoarsenates(V) with a mean value of 1.827 Å for 40 individual bond lengths within a AsO_6 group (Schwendtner, 2008), but apparently could not be realised in oxophosphates(V) which are known to contain solely tetrahedrally coordinated phosphorus atoms. A concise graphical representation of the modulation of the As_2O_7 group is depicted in Fig. 11.

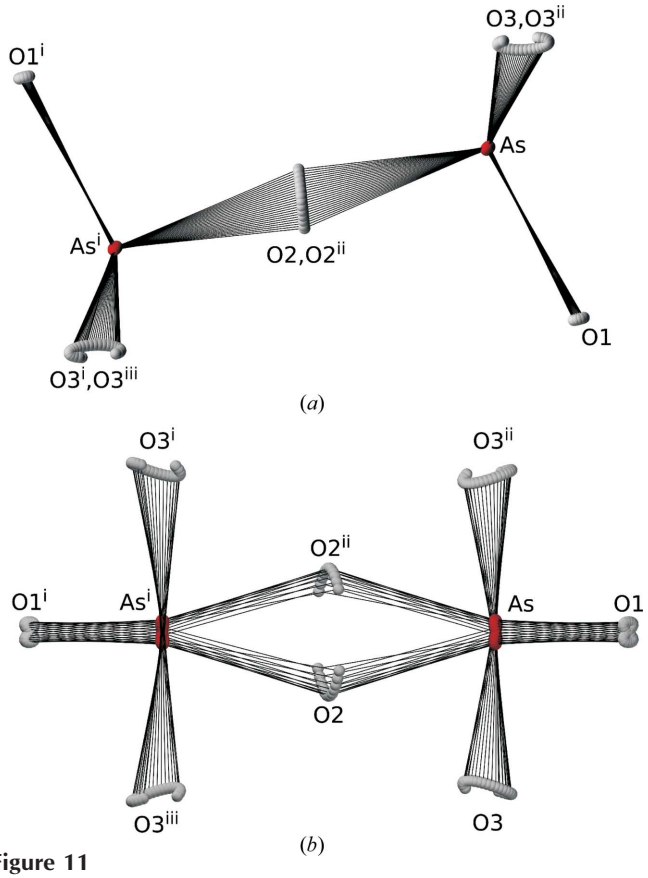

Figure 11
Graphical representation of the modulation of the As_2O_7 group of the β-$Zn_2As_2O_7$ structure using 25 equidistant t sections in the range t = [0,1], (*a*) viewed down [010] and (*b*) projected on (001). [Symmetry codes: (i) $-x_1+2, -x_2, -x_3+1, -x_4$; (ii) $x_1, -x_2, x_3, -x_4+\frac{1}{2}$; (iii) $-x_1+2, x_2, -x_3+1, -x_4+\frac{1}{2}$.]

Palatinus *et al.* (2006) have associated the incommensurability of the α_2-$Cr_2P_2O_7$ structure, which occurs as an intermediate between the low-temperature α_1-$Cr_2P_2O_7$ polymorph (285 K, α-$Zn_2P_2O_7$ structure type) and the high-temperature β-$Cr_2P_2O_7$ polymorph (345 K, thortveitite structure type), with the presence of low-symmetrical (bent) diphosphate groups in a rather high symmetry CrO_6 environment of the high-temperature phase, leading to a distortion of the α_2-$Cr_2P_2O_7$ structure. Another distortion, caused by the Jahn–Teller activity of Cr^{2+} with its d^4 electronic configuration, was discussed as an equally important factor. Zn^{2+}, on the other hand, has a d^{10} configuration which rules out any Jahn–Teller driven distortion of the ZnO_x polyhedra in α-$Zn_2As_2O_7$. However, what is common for both the intermediate α_2-$Cr_2P_2O_7$ and the high-temperature β-$Zn_2P_2O_7$ structure is the preference for coordination number 5 of some of the metal cations. Such behaviour makes them unique amongst other $M_2X_2O_7$ structures (M = Mg, 3d transition metals; X = P, As) where coordination number 5 is observed only for the low-temperature polymorphs α-$Cu_2P_2O_7$ (Robertson & Calvo, 1967) and α-$Zn_2P_2O_7$ (Robertson & Calvo, 1970), but never for the corresponding high-temperature polymorphs which all show coordination number 6 for the M^{2+} cations.

In summary, the interplay between the individual coordination sequences of the metal atoms within the metal oxide layers and the peculiar geometric features of the X_2O_7 groups appears to be the primary cause for the incommensurability of the α_2-$Cr_2P_2O_7$ and α-$Zn_2As_2O_7$ structures, but also seems to be responsible for the differences of the two structures.

4.2. A note on the crystal structure of petewilliamsite [(Ni,Co)$_2$As$_2$O$_7$]

In connection with the $M_2As_2O_7$ structures of 3d transition metals discussed in this article, the crystal structure of the mineral petewilliamsite must certainly be mentioned. Petewilliamsite has the idealized formula $(Ni,Co)_2(As_2O_7)$ and is the only pyroarsenate mineral characterized so far (Roberts *et al.*, 2004). As expected, the mineral possesses a thortveitite-type structure and its crystal structure was solved and refined in the space group $C2$, with Z = 30 and lattice parameters of a = 33.256 (5), b = 8.482 (1), c = 14.191 (2) Å and β = 104.145 (3)°. The relation between the C-centred thortveitite-type basic cell (subscript b) and the supercell (subscript s) is given by the relation

$$(\mathrm{Ni,\,Co})_2\mathrm{As}_2\mathrm{O}_7 : (\mathbf{a}_\mathrm{s}, \mathbf{b}_\mathrm{s}, \mathbf{c}_\mathrm{s}) = (\mathbf{a}_\mathrm{b}, \mathbf{b}_\mathrm{b}, \mathbf{c}_\mathrm{b}) \begin{pmatrix} 5 & 0 & 0 \\ 0 & 1 & 0 \\ 0 & 0 & 3 \end{pmatrix}; \quad \det(\boldsymbol{P}) = 15. \tag{4}$$

For the final structure model of petewilliamsite it was not possible to refine anisotropic displacement parameters for the mixed-occupied metal cation sites and the As atoms, or isotropic displacement parameters for the O atoms (Roberts *et al.*, 2004). Moreover, some of the AsO_4 tetrahedra exhibit

unrealistic bond lengths, either by being far too short (1.46 Å) or too long (2.02 Å) for tetrahedrally coordinated As. The reasons for such discrepancies in the structure model can be caused by a poorly diffracting crystal and/or weak superstructure reflections, consequently resulting in a low data-to-parameter-ratio, or may originate from unrecognized twinning. To shed light on the problems of the unsatisfactory petewilliamsite structure model, we have prepared polycrystalline material with nominal composition $(Ni,Co)_2As_2O_7$ by heating stoichiometric amounts of CoO, NiO and As_2O_5 in sealed silica tubes, followed by single-crystal growth using chemical transport reactions, as described in detail in §2. X-ray powder diffraction data (d values and intensities) of the obtained dark-red crystals are in good agreement with the data provided by Roberts *et al.* (2004) for the natural material. However, all grown crystals under investigation were non-merohedrally twinned by mirroring at (010). In each case, separation of the individual diffraction spots revealed triclinic cells very similar to that of α-$Ni_2As_2O_7$ with lattice parameters of $a \simeq 19.65$, $b \simeq 5.32$, $c \simeq 8.93$ Å, $\alpha \simeq 58.4$, $\beta \simeq 148.9$, $\gamma \simeq 127.2^\circ$, $V \simeq 384$ Å^3, which suggests that $(Ni,Co)_2As_2O_7$ is part of a solid solution series $(Ni_{1-x}Co_x)_2As_2O_7$ with $x \simeq 0.5$ based on α-$Ni_2As_2O_7$ as the parent ternary phase. The slight increase of the cell volume by $\sim 2\%$ conforms to an incorporation of the larger Co^{2+} into the structure of α-$Ni_2As_2O_7$ (ionic radius of high-spin Co^{2+} is 0.74 Å *versus* 0.69 Å for Ni^{2+}; Shannon, 1976). A satisfactory refinement of the $(Ni,Co)_2As_2O_7$ 'single-crystal' data based on the α-$Ni_2As_2O_7$ structure model was hampered by problems with separating the individual diffraction contributions of the respective twin domains during integration of the single-crystal intensity data. However, inspection of measured and simulated X-ray powder patterns assuming a mixed Co/Ni occupancy (ratio 1:1 for each metal site) showed satisfactory agreement, giving evidence that synthetic $(Ni,Co)_2As_2O_7$ adopts the α-$Ni_2As_2O_7$ structure type. Nevertheless, it cannot be excluded that the minor amount of Cu^{2+} present in natural petewilliamsite (about 8 mol%) is responsible for the formation of a 15-fold superstructure, as suggested by Roberts *et al.* (2004). Additional (powder and single-crystal) X-ray diffraction studies for a more reliable determination of the petewilliamsite structure with natural samples are currently in progress.

We would like to express our gratitude to Michal Dušek (Prague) for assistance with the refinement procedure of the incommensurately modulated structure of β-$Zn_2As_2O_7$. He, together with Vaclav Petříček (Prague) and Erich Zobetz (Vienna), also provided valuable comments on the manuscript. Uwe Kolitsch (Vienna) is acknowledged for additional X-ray data collections of single crystals on a Nonius Kappa-CCD diffractometer and Ekkehard Füglein (Netzsch GmbH) for some of the DSC measurements. BS thanks the Österreichische Forschungsgemeinschaft (ÖFG) for a MOEL stipend and the Czech Academy of Science for a 3-month stay in Prague.

References

Aranda, M. A. G., Bruque, S. & Attfield, J. P. (1991). *Inorg. Chem.* **30**, 2043–2047.
Baglio, J. A. & Dann, J. N. (1972). *J. Solid State Chem.* **4**, 87–93.
Becker, P. J. & Coppens, P. (1974). *Acta Cryst.* A**30**, 129–147.
Bergerhoff, G., Berndt, M., Brandenburg, K. & Degen, T. (1999). *Acta Cryst.* B**55**, 147–156.
Boudin, S., Grandin, A., Borel, M. M., Leclaire, A. & Raveau, B. (1993). *Acta Cryst.* C**49**, 2062–2064.
Bruker (2004). *SMART, RLATT* and *SAINT*. Bruker AXS Inc., Madison, Wisconsin, USA.
Bruker (2008). *TOPAS*4. Bruker AXS GmbH, Karlsruhe, Germany.
Bruker (2009). *APEX*2, *SAINT* and *SADABS*. Bruker AXS Inc., Madison, Wisconsin, USA.
Buckley, A. M., Bramwell, S. T. & Day, P. (1990). *J. Solid State Chem.* **86**, 1–15.
Buckley, A. M., Bramwell, S. T., Day, P. & Visser, D. (1995). *J. Solid State Chem.* **115**, 229–235.
Calvo, C. & Neelakantan, K. (1970). *Can. J. Chem.* **48**, 890–894.
Dowty, E. (2006). *ATOMS*, Version 6.3.1. Shape Software, 521 Hidden Valley Road, Kingsport, TN 37663, USA.
Effenberger, H. (1990). *Acta Cryst.* C**46**, 691–692.
Enraf–Nonius (1989). *CAD*4. Enraf–Nonius, Delft, The Netherlands.
Flack, H. D. (1983). *Acta Cryst.* A**39**, 876–881.
Flack, H. D. & Bernardinelli, G. (1999). *Acta Cryst.* A**55**, 908–915.
Glaum, R. (1999). Thesis of Habilitation (in German). University of Gießen, Germany; http://bibd.uni-giessen.de/ghtm/1999/uni/h990001.htm.
Gruehn, R. & Glaum, R. (2000). *Angew. Chem. Int. Ed.* **39**, 692–716.
Herrendorf, W. (1997). *HABITUS*. University of Gießen, Germany.
Hughes, M. & Brown, M. A. (1989). *Neues Jahrb. Miner. Monatsh.* pp. 41–47.
Li, L., Schönleber, A. & van Smaalen, S. (2010). *Acta Cryst.* B**66**, 130–140.
Lukaszewicz, K. (1963). *Bull. Acad. Pol. Sci. Chim.* **11**, 361–364.
Mercurio-Lavaud, D. & Frit, B. (1973). *C. R. Acad. Sci. C*, **277**, 1101–1104.
Palatinus, L., Dušek, M., Glaum, R. & El Bali, B. (2006). *Acta Cryst.* B**62**, 556–566.
Pertlik, F. (1980). *Monatsh. Chem.* **111**, 399–405.
Petříček, V. & Dušek, M. (2010). Personal communication.
Petříček, V., Dušek, M. & Palatinus, L. (2006). *JANA*2006. Institute of Physics, Praha, Czech Republic.
Petříček, V., van der Lee, A. & Evain, M. (1995). *Acta Cryst.* A**51**, 529–535.
Roberts, A. C., Burns, P. C., Gault, R. A., Criddle, A. J. & Feinglos, M. N. (2004). *Mineral. Mag.* **68**, 231–240.
Robertson, B. E. & Calvo, C. (1967). *Acta Cryst.* **22**, 665–672.
Robertson, B. E. & Calvo, C. (1970). *J. Solid State Chem.* **1**, 120–133.
Schäfer, H. (1964). *Chemical Transport Reactions*. New York: Academic Press.
Schwendtner, K. (2008). PhD thesis. University of Vienna, Austria.
Shannon, R. D. (1976). *Acta Cryst.* A**32**, 751–767.
Sheldrick, G. M. (2008). *Acta Cryst.* A**64**, 112–122.
Spek, A. L. (2009). *Acta Cryst.* D**65**, 148–155.
Stefanidis, T. & Nord, A. G. (1984). *Acta Cryst.* C**40**, 1995–1999.
van Smaalen, S. (1995). *Crystallogr. Rev.* **4**, 79–202.
Weil, M. (2001). *Acta Cryst.* E**57**, i28–i29.
Weil, M. (2004). *Acta Cryst.* E**60**, i139–i141.
Weil, M., Đorević, T., Lengauer, C. L. & Kolitsch, U. (2009). *Solid State Sci.* **11**, 2111–2117.
Weil, M., Lengauer, C. L., Füglein, E. & Baran, E. J. (2004*a*). *Cryst. Growth Des.* **4**, 1229–1235.
Weil, M., Lengauer, C., Füglein, E. & Baran, E. J. (2004*b*). *Z. Anorg. Allg. Chem.* **630**, 1768.
Zachariasen, W. H. (1930). *Z. Kristallogr.* **73**, 1–6.